JOURNAL OF GUIDANCE, CONTROL, AND DYNAMICS
Vol. 30, No. 2, March–April 2007

Continuous Thrust Orbit Transfer Optimization Using Large-Scale Linear Programming

Yuri Ulybyshev*
Rocket-Space Corporation "Energia," 141070, Korolev, Moscow Region, Russia

DOI: 10.2514/1.22642

A new technique is developed to optimize continuous medium- and low-thrust orbit transfers. This approach combines large-scale linear programming algorithms with discretization of the trajectory dynamics on segments and a set of pseudoimpulses or control for each segment. The set is a discrete approximation with a small mesh width for a space of possible thrust directions. Boundary conditions are presented as a linear matrix equation. A matrix inequality on the sum of characteristic velocities for the pseudoimpulses is used to transform the problem into a linear programming form. The number of decision variables is on the order of tens of thousands. In modern linear programming methods there are interior-point algorithms to solve such problems. In the general case, the continuous burns include a number of adjacent segments and a postprocessing of the linear programming solutions is needed to form a sequence of the burns. An optimal number of the burns is automatically determined in the postprocessing. A maintenance of a 24-hour elliptical orbit, long-term transfer from a geo-transfer to geostationary orbit, and a one-revolution, medium-thrust transfer between two elliptical noncoplanar orbits are considered as application examples. In the last two examples an iterative solution method was used. The presented method can be used effectively for trajectory optimization in a wide range of space missions.

Nomenclature

$\boldsymbol{A}$	=	matrix of inequality constraints, Eqs. (10) and (11)
$\boldsymbol{A}_e$	=	matrix of partial derivatives, Eq. (13)
a	=	semimajor axis, km
a_p	=	thrust acceleration, km/s^2
$\boldsymbol{b}$	=	vector of inequality constraints, Eq. (9)
E	=	eccentric anomaly
e	=	orbit eccentricity
$\boldsymbol{e}$, e_r, e_n, e_b	=	thrust direction unit vector and its components in local vertical/local horizontal coordinate system: radial, along-track, cross-track
$\boldsymbol{F}$	=	boundary condition function, Eq. (4)
h	=	energy integral
I	=	orbit inclination
i	=	segment number
J	=	performance index, Eq. (15)
j	=	pseudoimpulse number
k	=	quantity of pseudoimpulses at each segment
m	=	number of boundary conditions
n	=	quantity of segments
$\boldsymbol{P}_f$	=	vector of boundary conditions, Eq. (4)
$\boldsymbol{P}_f^*$	=	vector of boundary parameters along orbit without any maneuvers, Eq. (4)
p	=	orbit parameter
$\boldsymbol{q}$	=	weight coefficient vector of the fuel usage for the segments, Eq. (15)
$\boldsymbol{R}$	=	radius vector
t	=	time
U	=	argument of latitude
$\boldsymbol{V}$	=	spacecraft velocity vector
$\boldsymbol{X}$	=	vector of decision variables, Eq. (8)
$\Delta\boldsymbol{P}_f$	=	target vector, Eq. (12)
Δt_i	=	duration of ith segment
$\Delta V_i^{(j)}$	=	dimensionless characteristic velocity of jth pseudoimpulse at ith segment
ΔV_X	=	characteristic velocity
$\Delta\boldsymbol{V}_{Xi}$	=	characteristic velocity vector at ith segment
$\Delta\varphi$	=	angle between adjacent pseudoimpulses, Figs. 1 and 2
δV	=	characteristic velocity error, Fig. 2
$\delta\varphi$	=	thrust direction error, Fig. 2
λ	=	geodetic longitude of ascending node
μ	=	gravitational parameter for the Earth
φ	=	thrust yaw angle in local horizontal plane, Fig. 4
ω	=	mean orbit motion
ω_π	=	argument of perigee

I. Introduction

THE optimization of continuous thrust orbit transfers is an area of active research with a wide practical significance [1–11]. The optimal solutions in previous studies of medium- and low-thrust orbit transfer problems have been mainly of two types: indirect and direct

Yuri Ulybyshev graduated from the Bauman Moscow High Technical School [now the Bauman Moscow State Technical University (BMSTU)] in flight dynamics and control. Since 1977 he has worked in the Space Ballistics Department of the NPO "Energia" (now the Rocket-Space Corporation "Energia") and presently is head of the department. He has been involved in various space projects, such as the space shuttle Buran, the launch vehicle Energia, the spacecraft Soyz, the geostationary satellite Yamal, the space station Mir and International Space Station, the Sea Launch, and others. In 1990 he received his candidate of technical sciences degree (Ph.D) and in 2003 doctor of technical sciences degree (in the BMSTU). He has been recognized in *Who's Who in the World* (since 1998) and in *Who's Who in Science and Engineering* (since 2005). Currently he is also a lecturer professor in the BMSTU. His research interests include astrodynamics, spacecraft design, and control theory. He is a member of AIAA.

Received 23 January 2006; revision received 7 June 2006; accepted for publication 9 June 2006.

*Head of Space Ballistics Department; yuri.ulybyshev@rsce.ru. Member AIAA.

methods or their combinations. Indirect methods solve the classical optimal control problem by obtaining the solution to the corresponding two-point boundary value problem based on the Pontryagin maximum principle [12]. The boundary value problem can be solved numerically although it becomes a very difficult task for realistic problems because, in the general case, a good initial guess for unknown initial costate variables is usually not available. The direct approach is to discretize the original problem, transforming it into a parameter optimization problem, which is then solved using, as a rule, nonlinear programming methods [13]. Other interesting approaches are differential inclusions [14], feedback control [6,10], and genetic algorithms [3,4]. A current survey of space trajectory optimization methods was presented by Betts [15].

Linear programming represents one of the well-known optimization methods successfully used to solve many complex application problems in engineering, economics, and operations research. But the classical linear programming has not been practically used for orbit transfer optimization, in particular for continuous thrust transfers. The author knows only one paper [16] that deals with this problem. In a sense, the method of a linear convex correction proposed by Lidov [17] is related to this matter. The method was widely used for practical computations of rendezvous and orbit transfer trajectories in near-circular orbits [18]. Ulybyshev and Sokolov [7] have developed a method for optimization of many-revolution, low-thrust maneuvers in the vicinity of the geostationary orbit. The proposed mathematical model introduces pseudomaneuvers with either positive or negative transverse directions for every trajectory segment (half a revolution). This makes it possible to state the problem in terms of the classical linear programming with a number of decision variables equal to quadruple the number of revolutions in the orbit transfer.

In the 1990s, linear programming underwent a revolution with the development of polynomial-time algorithms known as interior-point methods [19–21]. The search directions for these methods strike out into the interior of the polytope rather than skirting around the boundaries, as do well-known simplex methods. Many studies now show that for large linear problems, the interior-point methods do better than classical simplex methods. Furthermore, unlike simplex-based algorithms that have difficulty with degenerate problems, interior-point methods are immune to degeneracy [20]. This makes it possible to develop methods that use large-scale linear programming for optimization of continuous thrust orbit transfers. The proposed methods are based on two ideas. The first is a known discretization of the transfer time on, in the general case, nonuniform segments. The second is the key idea based on a near-uniform discrete approximation of a control space by a set of pseudoimpulses with an inequality constraint for each segment.

A numerical efficiency of the methods is demonstrated by considering three application examples. The first problem is the maintenance of a 24-hour elliptical orbit. It is an optimization of station-keeping maneuvers in a neighborhood of the orbit for a spacecraft with possible thrust directions in a local horizontal plane. The second and third problems are examples of general noncoplanar orbit transfers with thrust directions in a plane and three-dimensional space, respectively. For these, we use an iterative method including a linear programming solution sequence.

The contribution of the paper is a demonstration that the presented technique, in spite of a high order, shows an effectiveness and robustness, and hence, is a good candidate for optimization and analysis of continuous thrust orbit transfers and perhaps other applications.

II. Continuous Thrust Orbit Transfer

A. Motion Equations

We consider a point-mass spacecraft with a constant thrust acceleration $0 \le a_p \le a_{p\max}$. The equations of the spacecraft motion in an inverse-square gravity field are given

$$\frac{\mathrm{d}\boldsymbol{Y}}{\mathrm{d}t} = \boldsymbol{f}[\boldsymbol{Y}(t), a_p(t), \boldsymbol{e}(t)] \tag{1}$$

where

$$\boldsymbol{Y}^{\boldsymbol{T}}(t) = [\boldsymbol{r}^{\mathbf{T}}(t), \boldsymbol{V}^{\boldsymbol{T}}(t)] \tag{2}$$

and

$$\boldsymbol{f}[\boldsymbol{Y}(t), a_p(t), \mathbf{e}(t)] = \begin{Bmatrix} \boldsymbol{V}(t) \\ a_P(t)\boldsymbol{e}(t) - \frac{\mu \boldsymbol{r}(t)}{r^3(t)} \end{Bmatrix} \tag{3}$$

where $\boldsymbol{r}(t)$, $\boldsymbol{V}(t)$ are the radius vector and velocity vector, respectively. Here $\boldsymbol{e}$ denotes the thrust direction unit vector ($\boldsymbol{e}^T \cdot \boldsymbol{e} \equiv 1$).

Orbit transfer boundary conditions are

$$\boldsymbol{F}[\boldsymbol{Y}(t_{f1}), \boldsymbol{Y}(t_{f2}), \ldots, \boldsymbol{Y}(t_f)] = \boldsymbol{P}_f \tag{4}$$

where $\boldsymbol{F}$ is a vector function of a state vector at the final time and, in the general case, at interior points of the transfer t_{f1}, t_{f2}, etc.; $\boldsymbol{P}_f$ is an m-dimension specified vector of the boundary conditions.

B. Time Discretization

Introduce the partition $[t_0, t_1, t_2, \ldots, t_n]$, with $t_0 = 0$ and $t_n = t_f$, and $t_0 < t_1 < t_2 \ldots < t_n$, and let $\Delta t_i = t_{i+1} - t_i$ be a small time interval for $i = 1, 2, \ldots, n$. The mesh points t_i are referred to as nodes; the intervals $[t_{i+1}, t_i]$ are referred to as trajectory segments. In the general case, the segments can be nonuniform. Suppose that $\boldsymbol{Y}(t)$ is approximated by values at the nodes, then for a constant control $\boldsymbol{a}_i = a_p \boldsymbol{e}_i$ at each segment, we can write

$$\boldsymbol{P}_f = \boldsymbol{P}_f^* + \sum_{i=1}^{n} \Delta \boldsymbol{F}(\boldsymbol{Y}_i, a_p, \boldsymbol{e}_i, \Delta t_i) \tag{5}$$

where $\boldsymbol{P}_f^*$ is a vector of the boundary parameters computed along an orbit without any maneuvers; $\Delta \boldsymbol{F}$ is a change of the boundary conditions at the ith segment. In a sense, Eq. (5) represents a simple form of the well-known Encke's method [22], which uses integration of only the difference from a reference orbit whose ephemeris is known.

Note that the final transfer time t_f and segment duration Δt_i may be defined in an implicit form. It may be a number of revolutions or function of time, argument of latitudes, orbital elements, etc.

III. Orbit Transfer Problem in Linear Programming Form

A. Large-Scale Linear Approximation of Control

As the first case, we describe a control problem with a thrust vector in a plane. As an example, it can be a local horizontal or orbit plane. We consider an ith segment independent of all the other segments. The thrust direction in the plane is arbitrary. Without loss of generality, let a dimensionless characteristics velocity or impulse for the segment be $\Delta V_{i\max} = 1$. The possible thrust directions can be present as a set of pseudoimpulses within the unit circle with a small angle of $\Delta\varphi = 2\pi/k$ between them (Fig. 1a). Suppose that there is an optimal impulse $\Delta \mathbf{V}_{i\mathrm{opt}}$ for the ith segment. Thus we can replace the optimal impulse by an approximating form as a constrained sum of the characteristic velocities of the pseudoimpulses (Fig. 1b):

$$\Delta V_i^{(1)} + \Delta V_i^{(2)} + \ldots + \Delta V_i^{(k)} \le \Delta V_{i\max} \equiv 1 \tag{6}$$

It is evident that an optimal vector approximation of the optimal impulse by pseudoimpulses is a sum of the two nearest neighbor pseudoimpulses. In a particular case, it can be one nearest neighbor pseudoimpulse. An error of this approximation for the characteristic velocity δV depends on an angle of $\Delta\varphi$ We can write (Fig. 2)

$$\boldsymbol{e}\,(1 - \delta V) = \Delta V_i^{(j)} \boldsymbol{e}_j + \Delta V_i^{(j-1)} \boldsymbol{e}_{j-1} \tag{7a}$$

or

$$\delta V = 1 - \Delta V_i^{(j)} \cos\delta\varphi - \Delta V_i^{(j-1)} \cos(\Delta\varphi - \delta\varphi) \tag{7b}$$

where $\Delta V_i^{(j)} + \Delta V_i^{(j-1)} = 1$. Simple computations show that δV is very small and for arbitrary values $\Delta V_i^{(j)}$, $\Delta V_i^{(j-1)}$, and $\delta\varphi$, it is no more than 0.5×10^{-3} and 4×10^{-3}, respectively, for $\Delta\varphi = 2$ deg and $\Delta\varphi = 5$ deg.

By a similar way, we consider a three-dimensional case for possible thrust directions. A set of pseudoimpulses can be constructed using a uniform distribution on a unit sphere based on computational geometry methods. An example of a mesh with $k = 1000$ points on the sphere is depicted in Fig. 3. Similarly to the planar case, for each segment, the sum of characteristic velocities of the pseudoimpulses should be constrained by an inequality defined by Eq. (6). The best approximation of an optimal impulse $\Delta \boldsymbol{V}_{i\text{opt}}$ is also a sum of nearest neighbor pseudoimpulses. For the mesh, the angles between the adjacent pseudoimpulses are no more than 3 deg. As in the planar case, δV is of order 1×10^{-3}.

Define a $(n \times k)$-dimension vector of decision variables

$$\boldsymbol{X}^T = [\Delta V_1^{(1)}, \Delta V_1^{(2)}, \ldots \Delta V_1^{(k)}, \Delta V_2^{(1)}, \Delta V_2^{(2)}, \ldots \Delta V_2^{(k)}, \ldots \Delta V_n^{(k)}] \tag{8}$$

It should be noted that all the vector components must be nonnegative. For the vector, according to the previous statements, the following linear inequality can be written:

$$\boldsymbol{AX} \le \boldsymbol{b} \tag{9}$$

where $\boldsymbol{A}$ is a $n \times (n \times k)$-dimension matrix of the following form (all of the unspecified elements equal to zero):

$$\boldsymbol{A} = \underbrace{\left[\begin{array}{cccc} \underbrace{111\ldots1}_{k} & & & \\ & 111\ldots1 & & \\ & & 111\ldots1 & \\ & & & 111\ldots1 \end{array}\right]}_{n\times k} \Bigg\}n \tag{10}$$

and a n-dimension vector $\boldsymbol{b^T} = [1, 1, \ldots 1]$.

Real space missions, especially for spacecraft using electric propulsion, are often required to satisfy constraints related to an engine time of $\Delta t_{R\max}$ at time subintervals. In our problem, the additive constraints are required for a quantity of the adjacent segments corresponding to the subintervals. An example of the matrix $\boldsymbol{A}$ and vector $\boldsymbol{b}$ for N segments at each subinterval is

$$\boldsymbol{A} = \left[\begin{array}{ccccccccccc} \underbrace{11\ldots1}_{k} & \ldots & & & & & & & & & \\ & & \underbrace{11\ldots1}_{k} & & & & & & & & \\ & & & \underbrace{11\ldots1}_{k} & \ldots & & & & & & \\ & & & & & \underbrace{11\ldots1}_{k} & \ldots & & & & \\ & & & & & & & \underbrace{11\ldots1}_{k} & \ldots & & \\ & & & & & & & & & \underbrace{11\ldots1}_{k} & \\ \underbrace{\Delta t_{1\max}\ldots\Delta t_{1\max}}_{Nxk} & & & & & & & & & & \\ & & \underbrace{\Delta t_{2\max}\ldots\Delta t_{2\max}}_{Nxk} & & & & \ldots & & & & \\ & & & & & & & & & \underbrace{\Delta t_{s\max}\ldots\Delta t_{s\max}}_{Nxk} & \end{array}\right] \begin{array}{l} \Big\} \text{basic constraints for pseudoimpulses} \\ \Big\} \text{additive constraints} \end{array} \tag{11a}$$

$$\boldsymbol{b}^T = [\overbrace{1, 1, \ldots 1}^{\text{basic constraints for pseudoimpulses}}, \overbrace{\Delta t_{R\max}, \ldots, \Delta t_{R\max}}^{\text{additive constraints}}] \tag{11b}$$

B. Transformation to Linear Programming Form

For the decision variable vector $\boldsymbol{X}$, the boundary conditions from Eq. (5) can be expressed as

$$\Delta \boldsymbol{P}_f = \boldsymbol{P}_f - \boldsymbol{P}_f^* = \boldsymbol{A}_e \boldsymbol{X} \tag{12}$$

where $\Delta \boldsymbol{P}_f$ is a target vector, $\boldsymbol{A}_e$ is a $m \times (n \times k)$-dimension matrix of partial derivatives

$$\boldsymbol{A}_e = \left[\begin{array}{cccccccc} \frac{\partial F_1}{\partial V_1^{(1)}} & \frac{\partial F_1}{\partial V_1^{(2)}} & \cdots & \frac{\partial F_1}{\partial V_1^{(k)}} & \frac{\partial F_1}{\partial V_2^{(1)}} & \cdots & \frac{\partial F_1}{\partial V_n^{(k)}} \\ \frac{\partial F_m}{\partial V_1^{(1)}} & \frac{\partial F_m}{\partial V_1^{(2)}} & \cdots & \frac{\partial F_m}{\partial V_1^{(k)}} & \frac{\partial F_m}{\partial V_2^{(1)}} & \cdots & \frac{\partial F_m}{\partial V_n^{(k)}} \end{array}\right] \tag{13}$$

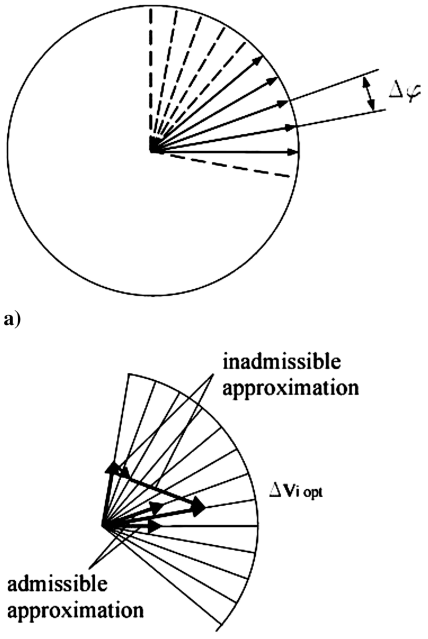

Fig. 1 Set of pseudoimpulses in a plane.

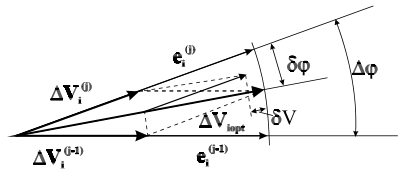

Fig. 2 Approximation of optimal solution for *i*th segment.

where $\partial F_q / \partial V_i^{(j)}$ is a partial derivative. For partial derivatives with a linear dependence on the segment duration it is

$$\frac{\partial F_q}{\partial V_i^{(j)}} = a_p \Delta t_i \frac{\partial F_q}{\partial \boldsymbol{a}_p} \boldsymbol{e}_j \tag{14}$$

However, for a nonlinear dependence, the partial derivatives can be computed as changes of the boundary conditions at the corresponding segments for maximum durations. Further, it requires refinements. A corresponding example will be presented next.

Introduce a $(n \times k)$-dimension vector of weight coefficients as $\boldsymbol{q}^T = [1 \quad 1 \ldots 1 \quad 1]$ for the equal segments or as $\boldsymbol{q}^T = [\Delta t_{1\max} \ldots \Delta t_{n\max}]$ for unequal segments. Then, a performance index corresponding to the minimum characteristic velocity of the transfer can be written as

$$J = \min(\boldsymbol{q}^T \cdot \boldsymbol{X}) \tag{15}$$

As a result, we have a classical linear programming problem with constraints of a linear inequality and equality given by Eqs. (9) and (12), respectively. The elements of the decision variable vector $\boldsymbol{X}$ must be nonnegative and constrained

$$0 \le \Delta V_i^{(j)} \le 1 \tag{16}$$

It should be noted that it is a large-scale problem. As an example, for a many-revolution orbit transfer with 30 revolutions, 36 segments in each revolution, and 36 pseudoimpulses, the number of decision variables is (30 revolutions × 36 segments × 36 pseudoimpulses) =38, 880. The matrix $\boldsymbol{A}$ has dimension $1440 \times 103,680$. But it is a sparse matrix with a low number of nonzero elements (for the example, it is ∼0.1%). Modern scientific software, such as the MATLAB®, have effective algorithms for sparse matrix computations [23] including large-scale linear programming.

It is evident that the segments in the linear programming form are formally considered independent of each other. Therefore, additional postprocessing and validation are required for the linear programming solutions. It is necessary to find all of the segments corresponding to the nonzero decision variables (more exactly, corresponding to the variables no less than a computation error of order δV). The adjacent segments among these should be joined in burns. If two (or three in the three-dimensional case) decision variables belong to a segment then the thrust magnitude and direction should be computed from the vector sum of the corresponding pseudoimpulses (see Fig. 2). As is well known from primer vector theory [24–26], nonsingular optimal space trajectories must be formed by intervals of maximum thrust and coast arcs separated by a finite number of switches, and the optimal thrust direction is always aligned with the primer vector. By this is meant that the characteristic velocity for the segments of a burn must correspond to $\Delta V_{i\max}$ (with a relative error of order δV). The exceptions are only the first and last segments in the burn. A noncompliance with these qualitative properties for optimal transfer trajectories may indicate that it is a singular solution. For an inverse-square gravity field, the primer vector is a function of the eccentric anomaly with periodic and secular terms. Therefore the thrust direction rate in the burn must be of the same order as the orbital angular velocity, and high-frequency chattering should be lacking. To our knowledge, for a general continuous thrust orbit transfer case, determination of the optimal number of burns is an unsolved problem. We believe that it is no more than 4–6 burns per one revolution. In the proposed method the optimal number of burns is automatically determined in the postprocessing. Our computational experience shows that if a linear programming solution satisfying the boundary conditions exists then the postprocessing solution does not collide with the cited qualitative properties of the theory of optimal space trajectories. If the segments are the possible burn arcs, then the described validation is not required. Furthermore, optimal solutions can be included burns with nonmaximal characteristic velocities.

The interior-point methods are not only highly efficient algorithms for the large-scale linear programming, but they are immune to degeneracy [20]. Therefore the absence of a solution means, most likely, that the thrust acceleration (i.e., the spacecraft thrust-to-weight ratio) is small for the orbit transfer, or the problem formulation with the boundary conditions and constraints is degenerate. For the last case, an attempt of solution for a very high-thrust acceleration can be used as a validation test of the possible degeneracy.

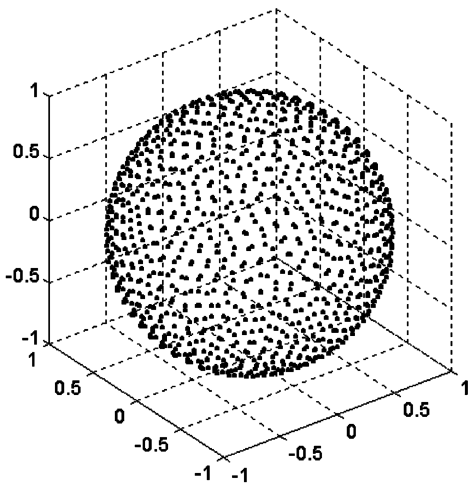

Fig. 3 Near-uniform point distribution on unit sphere, 1000 points.

C. On Orbital Maneuvers Categories

In a sense, the orbital maneuvers can be divided into two categories: orbit station-keeping and orbit transfers. The station-

keeping uses nearly continual or periodic maneuvers to maintain a reference orbit, which has continuous perturbations (Earth's gravity harmonics, moon-sun gravitational attraction, atmospheric drag, solar radiation pressure). As a rule, the station-keeping maneuvers performed in a neighborhood of the reference orbit and the partial derivatives in Eq. (13) are known with relatively high precision.

Further, the orbit transfers can be conditionally categorized into two classes: long-term or many-revolution transfers and short-term, as an example one-revolution, transfers. By contrast the station-keeping for both orbit transfer classes, an intermediate transfer orbit and, respectively, the partial derivatives in Eq. (13), are usually not known a priori. For this case, we can use an iterative technique with a refinement of the partial derivatives at each iteration. For the first iteration we define an initial guess for the intermediate orbit parameters. As an example, it can be a linear time variation between initial and target orbits. Based on the linear programming solution, the parameters are refined for the second iteration, etc., to satisfy the specified boundary conditions.

For continuous thrust orbit transfers, the optimal control techniques in the form of an iterative solution for a two-point boundary value problem for the state and adjoint variables are difficult to apply. The main difficulty with these methods is getting started, i.e., finding a first estimation of the unspecified conditions for the state and adjoint variables [27]. Moreover, the adjoint variables do not have a physical meaning, and thus, it can be difficult to find a reasonable initial guess for them. Contrary to these techniques, in an iterative process for the proposed method, unknown orbital elements of the intermediate orbit have, as a rule, monotonic variations and known variation ranges between elements of the initial and final orbits.

IV. Application Examples

A. Long-Term Station-Keeping of 24-Hour Elliptical Orbit

As an example of an orbit maintenance problem, we consider a 24-hour high altitude elliptical orbit for the Sirius Satellite Radio [28]. Orbital elements of the orbit are shown in Table 1.

It is a geosynchronous critically inclined orbit with perigee at the southern hemisphere which the argument of perigee remains nearly constant. This allows it to be fixed over the high-latitude areas of the northern hemisphere and makes such an orbit well suited for communications.

The long-term evolution of the orbit due to the Earth's nonspherical potential, sun and moon gravity, and solar radiation pressure is very complex. An additional perturbation affecting a ground track of the orbit is due to resonance with longitude terms in the Earth's gravity potential because the ground track is repetitive every day. Station-keeping goals include maintaining the orbital elements of I, w_π, and e near to their nominal values and the geodetic longitude of the ascending node λ_N, within a box of ± 1 deg. A priori analysis of the orbit evolution has shown that I, w_π, and e are slow variables and λ_N is a relatively fast variable. The orbital elements and λ_N are used as controlled parameters. Boundary conditions for λ_N was assigned not only at a final time for a station-keeping interval, but at interior-points of the interval. An explicit control for the orbital period is not needed because it is maintained through the ground track control.

A spacecraft with a very low-thrust acceleration of $a_p = 1 \times 10^{-8}$ km/s^2 and possible thrust directions in the local horizontal plane (Fig. 4) was considered. The station-keeping interval duration

Table 1 Nominal orbital elements

Parameter	Value
Orbit period, s	86,164
Inclination I, deg	63.4
Eccentricity e	0.27
Argument of perigee ω_π, deg	270

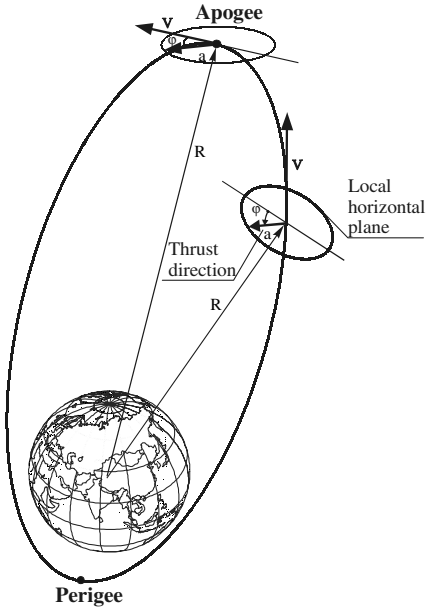

Fig. 4 Thrust direction in local horizontal plane.

was $N_{\text{REV}} = 30$ revolutions (it is near to one month). Interior-point constraints for λ_N were assigned after 10 and 20 revolutions.

Therefore a vector of the boundary conditions is $\boldsymbol{P}_f^{\boldsymbol{T}} = [I, \omega_\pi, e, \lambda_{N10}, \lambda_{N20}, \lambda_{N30}]$. The partial derivatives based on Gauss's form of the variational equations [22] for an ith segment and jth pseudoimpulse can be written as

$$\frac{\partial I}{\partial V_i^{(j)}} = \frac{r_i \cos(u_i)}{h} \sin(\varphi_j) a_p \Delta t_i \tag{17}$$

$$\frac{\partial \omega_\pi}{\partial V_i^{(j)}} = \frac{1}{h}\left[\frac{(p + r_i)\sin(\vartheta_i)\cos(\varphi_j)}{e} - \frac{r_i \sin(u_i)\cos(I)\sin(\varphi_j)}{\sin(I)}\right] a_p \Delta t_i \tag{18}$$

$$\frac{\partial e}{\partial V_i^{(j)}} = \frac{1}{h}[(p + r_i)\cos(u_i) + r_i e]\cos(\varphi_j) a_p \Delta t_i \tag{19}$$

where $h = \sqrt{\mu p}$, $p = a(1 - e^2)$, Δt_i is the segment duration, $u_i = \omega_\pi + \vartheta_i$ is the argument of latitude, and, ϑ_i is the true anomaly for the beginning of the segment. The partial derivative for the geodetic longitude of the ascending node is

$$\frac{\partial \lambda_N}{\partial V_i^{(j)}} = \frac{\partial \lambda_N(t_i)}{\partial T} \cdot \frac{\partial T}{\partial a} \cdot \frac{\partial a}{\partial V_i^{(j)}} \tag{20}$$

where

$$\frac{\partial \lambda_N}{\partial T} = -\omega_z (t_f - t_i)/T \tag{21}$$

$$\frac{\partial T}{\partial a} = \frac{-3\pi\mu}{a^4 \sqrt{\mu/a^3}} \tag{22}$$

$$\frac{\partial a}{\partial V_i^{(j)}} = \frac{2a^2 p}{h r_i} \cos(\varphi_j) a_p \Delta t_i \tag{23}$$

where t_f is the final time and w_z is the Earth's rotation rate. Note that the partial derivatives are linear functions of a segment duration.

For elliptical orbits, a discretization with the segments uniform in the true anomaly is more preferable. We used $n_{\text{REV}} = 36$ segments in one revolution and 36 pseudoimpulses in each segment. The number

of burns in one revolution is not specified, but the total engine time for all such subintervals is constrained by $\Delta t_{R\max} \le 6$ h. Thus, we have $n = N_{\text{REV}} \times n_{\text{REV}} = 1080$ segments, a $n \times k = 38,880$ dimension vector of the decision variables, and a $(n + N_{\text{REV}}) \times L = 1110 \times 38,880$ dimension matrix of the inequality constraints (all of the unspecified elements equal to zero).

Initial values for the orbit propagation correspond to the nominal orbital elements from Table 1 at the ascending node, $\lambda_N = 0$, and an epoch of 1 January 2008, 0 hrs UTC. Simulation results of solutions for 12 successive maintenance intervals (summary near to 1 year) are given in Fig. 5. These are time histories (the bold lines) for the geodetic longitude of the ascending node λ_N (Fig. 5a), orbit inclination I (Fig. 5b), argument of perigee w_π (Fig. 5c), and eccentricity e (Fig. 5d). For comparison, evolutions of the elements without any maneuvers are displayed by the thin lines. Wide variations of required characteristic velocities mainly depend on the moon–sun gravity perturbations. For the one-month station-keeping it is $\Delta V_{X\text{MONTH}} = 2.9$–$7.9$ m/s. The 1 year total characteristic velocity is $\Delta V_{X\text{YEAR}} = 58$ m/s. It compares well with a high-thrust propulsion system for orbit maintenance [28] where $\Delta V_{X\text{YEAR}} = 35$–$80$ m/s. Examples of the burns distribution vs revolution are shown in Figs. 6 and 7 for months 3 and 12, respectively, for the minimal and maximal required $\Delta V_{X\text{MONTH}}$. Each burn is depicted as a gray-filled rectangle with a height equal to the burn duration. Gray colors of the rectangles correspond to required yaw angles of the burns in compliance with the color axis scaling (the right side of Figs. 6 and 7). It is shown that the distribution of the burn durations at the revolutions is irregular. The maximum number of the burns in a revolution is three. Note that, for months with intensive maneuvers, the total engine time in one

$$
\boldsymbol{A} = \begin{bmatrix}
\underbrace{11\ldots1}_{k=36} & \cdots & \underbrace{11\ldots1}_{k=36} & \cdots & \underbrace{11\ldots1}_{k=36} & \cdots & \underbrace{11\ldots1}_{k=36} \\
\underbrace{\Delta t_{1\max}\Delta t_{2\max}\ldots\Delta t_{(n_v\times k)}}_{n_{\text{REV}}\times k=1080} & & & & & & \\
 & & & \cdots & & & \underbrace{\Delta t_{\mu\max}, \Delta t_{\mu+1\max}\ldots t_{j\max}}_{n_{\text{REV}}\times k=1080}
\end{bmatrix} \tag{24}
$$

A $n + N_{\text{REV}}$-dimension vector of inequality constraints is $\boldsymbol{b}^T = [1 \quad 1\ldots1 \quad \Delta t_{R\max}\ldots\Delta t_{R\max}]$.

To test the performance of the proposed method, a code has been written for simulation of the station-keeping problem for the orbit affected by the perturbations. The truth orbit is propagated by numerically integration of motion equations with the Earth's gravitational field (12×12 GEM-T2 model [29]), sun and moon gravity, and solar radiation pressure. As the initial step, we compute the boundary parameters $\Delta \boldsymbol{P}_f^*$ for the orbit without any maneuvers. Further, at the first iteration, a linear programming solution was found for the target vector $\Delta \boldsymbol{P}_f^{(1)}$ from Eq. (12). After the postprocessing we compute a new trajectory with the burns and calculate a target vector displacement from zero $\delta \boldsymbol{P}_f$. For the second iteration, the target vector is refined as $\Delta \boldsymbol{P}_f^{(2)} = \Delta \boldsymbol{P}_f^{(1)} + \delta \boldsymbol{P}_f$, etc. As a rule, to obtain a converged solution, only four or five iterations are needed in this computation. The matrix of the partial derivatives $\boldsymbol{A}_e$ from Eq. (13) are computed only once along the reference orbit. It is a simple form of shooting method for boundary value problems [15].

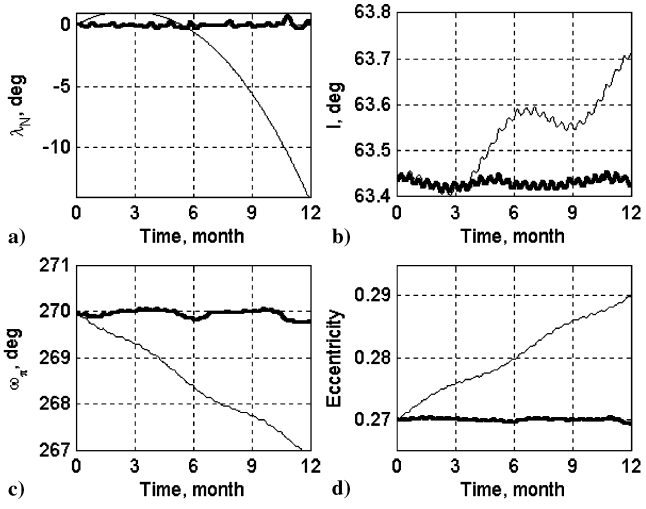

Fig. 5 Orbital elements histories.

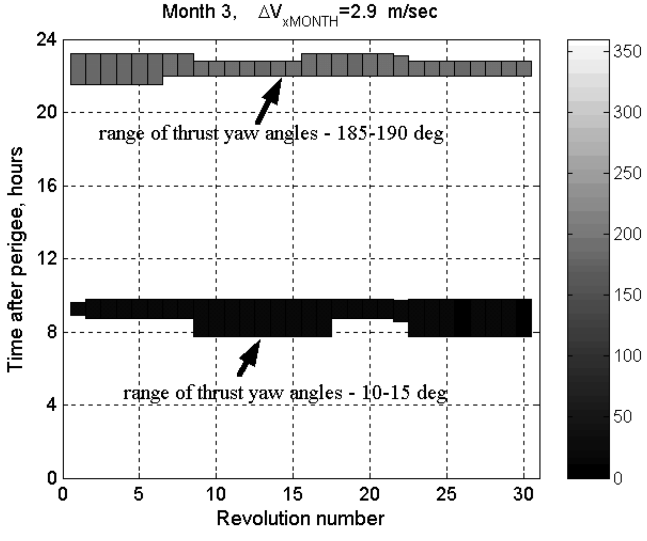

Fig. 6 Example distribution of low-intensity maneuvers.

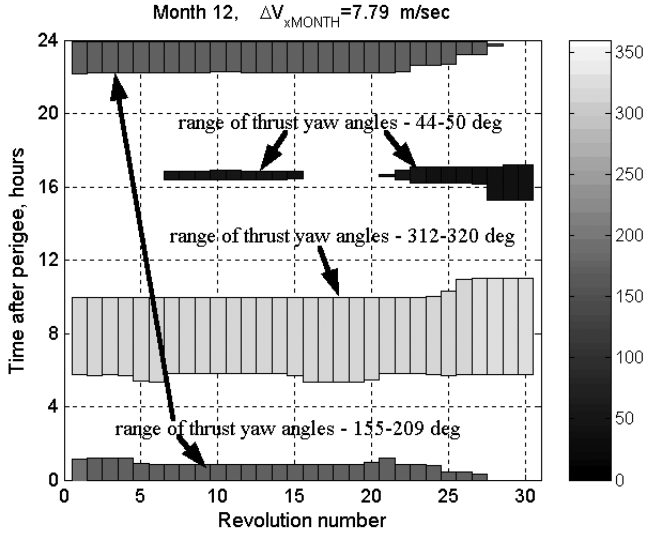

Fig. 7 Example distribution of intensity maneuvers.

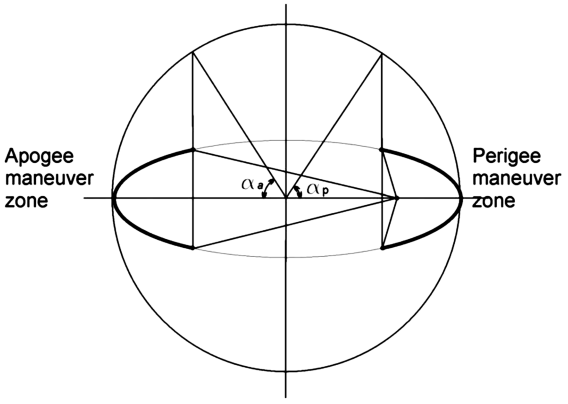

Fig. 8 Burn arcs at elliptical orbit.

revolution is an active constraint and results in a redistribution of burns between revolutions. Most burns are grouped near apogee or perigee.

B. Many-Revolution Orbit Transfer

An effective method for computation of long-term orbit transfers is to use an averaging technique that ignores the short-term variations of the orbital elements [8]. In this case the secular rate of one element

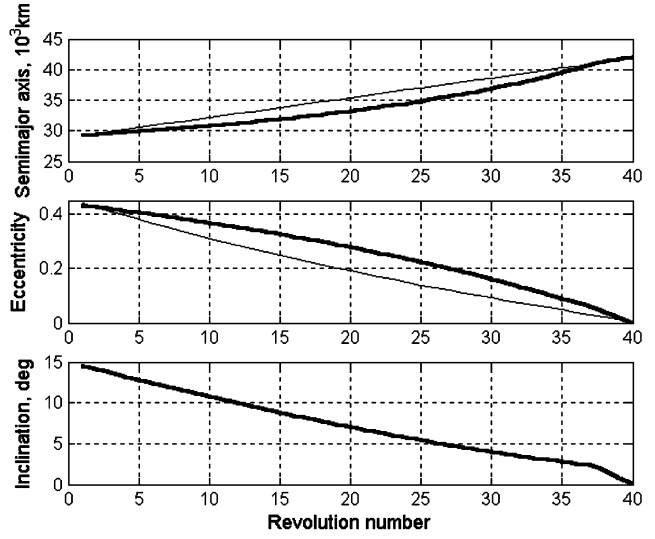

Fig. 9 Orbital elements histories.

Table 2 Orbit transfer parameters

Orbit	a, km	I, deg	E	ω_π, deg
Initial	16,378	50	0.1	30
Target	26,378	60	0.2	90

change is calculated by holding the others constant over one revolution. As in [8], assume it possible to have perigee- and apogee-centered burn arcs in each revolution (Fig. 8) and, as in the previous example, the thrust directions lie in the local horizontal plane (Fig. 4). The segments are these burn arcs. Then the number of segments is equal to double the number of revolutions for the orbit transfer.

Suppose that a spacecraft with a constant thrust acceleration of $a_p = 1.5 \times 10^{-6}$ km/s^2 is in an elliptical geo-transfer orbit (GTO) with a semimajor axis of $a = 29,721$ km, an eccentricity $e = 0.44$, and an inclination $I = 15$ deg. The maximum lengths of the burn arcs are defined by angles $\alpha_p = 90$ deg for the perigee and $\alpha_a = 40$ deg for the apogee (Fig. 8). A vector of the boundary conditions for a final geostationary orbit (GEO) is $\boldsymbol{P}_f^T = [a_f, e_f, I_f] = [42, 164.16 \text{ km}, 0, 0]$. Based on equations for secular rates of orbital element changes [8], the partial derivatives for an ith segment and jth pseudoimpulse can be expressed as

$$\frac{\partial a}{\partial V_i^{(j)}} = \frac{2a_p}{\pi}\sqrt{\frac{a_i^3}{\mu}(1-e_i^2)}\alpha\cos(\varphi_j) \tag{25}$$

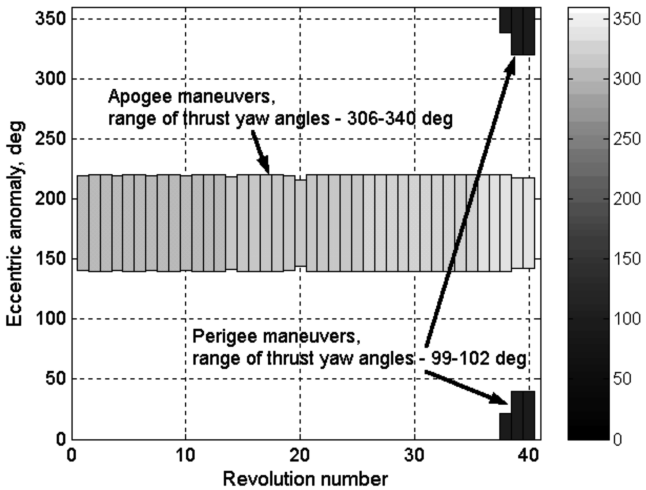

Fig. 10 Maneuver distribution.

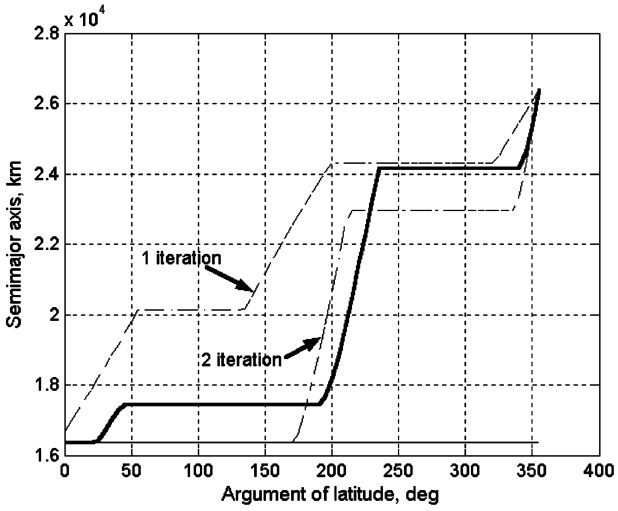

Fig. 11 Semimajor axis history.

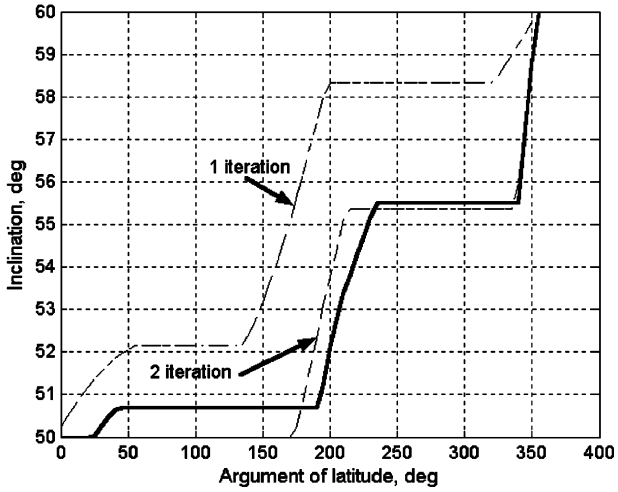

Fig. 12 Inclination history.

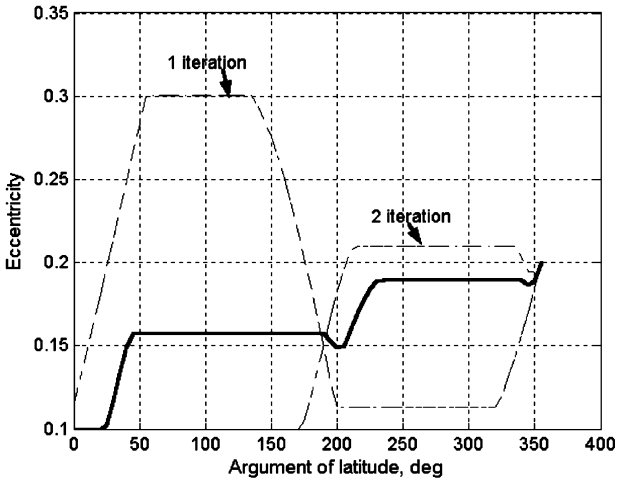

Fig. 13 Eccentricity history.

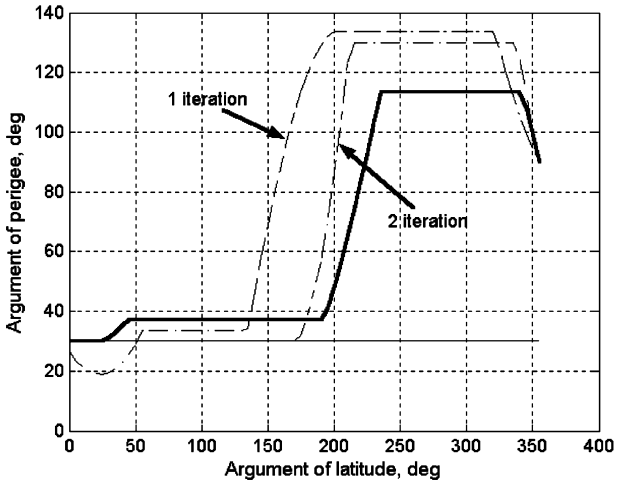

Fig. 14 Argument of perigee history.

$$\frac{\partial e}{\partial V_i^{(j)}} = -\frac{a_p}{2\pi}\sqrt{\frac{a_i^3}{\mu}(1-e_i^2)}(4\sigma\sin\alpha + 3e_i\alpha + e_i\cos\alpha\sin\alpha)\cos(\varphi_j) \tag{26}$$

$$\frac{\partial I}{\partial V_i^{(j)}} = -\frac{a_p}{2\pi}\sqrt{\frac{a_i}{\mu}}\cos\omega_{\pi i}G_i(\sigma,\alpha,e_i)\sin(\varphi_j) \tag{27}$$

where

$$G_i(\sigma,\alpha,e_i) = \frac{2\sigma\sin\alpha(1+e_i^2) + 3e_i\alpha + e_i\cos\alpha\sin\alpha}{\sqrt{1-e_i}} \tag{28}$$

$$\omega_{\pi i} = \omega_{\pi i-1} - \frac{a_p}{2\pi}\sqrt{\frac{a}{\mu}}\cot(I_{i-1})\sin(\omega_{\pi i-1})G(\sigma,\alpha,e_{i-1}) + A(a_{i-1},e_{i-1},I_{i-1}) \tag{29}$$

$$A(a,e,I) = \frac{\mathrm{d}\omega}{\mathrm{d}t} = \frac{3}{4}J_2\left(\frac{R_e}{p}\right)^2\omega(4-5\sin^2 I_{i-1}) \tag{30}$$

Table 3 Example for postprocessing of linear programming solution

Linear programming solution							Postprocessing data				
Nonzero decision variables	ΔV_{xi}, m/s	Segment duration Δt_i, s	Segment number	Thrust unit vector elements			Maneuver number	Begin time of burn, s	Burn duration, s	ΔV_x, m/s	$\Delta\gamma$, deg
				e_r	e_n	e_b					
0.1784	8.4	42	6	0.8116	−0.1866	0.5535					
1	47.2	236	7	0.8116	−0.1866	0.5535					
1	47.2	236	8	0.8668	−0.1013	0.4882	1	1385	853	170.6	11.6
1	47.4	237	9	0.8668	−0.1013	0.4882					
0.4290	20.4	102	10	0.9124	−0.1457	0.3824					
0.5182	47.1	235	40	0.5126	0.2366	−0.8254					
1	92.1	461	41	0.5999	0.2511	−0.7596					
1	90.7	454	42	0.7013	0.2432	−0.6701					
1	87.5	438	43	0.7756	0.2583	−0.5760					
1	88.2	441	44	0.8379	0.2662	−0.4765	2	11205	3938	787.4	30.8
1	91.5	457	45	0.8379	0.2662	−0.4765					
1	94.9	475	46	0.7730	0.3659	−0.5182					
1	98.6	493	47	0.7730	0.3659	−0.5182					
0.9465	96.8	484	48	0.82840	0.3710	−0.4197					
1	125.4	627	70	0.3000	−0.2584	0.9183					
1	119.3	596	71	0.4290	−0.3041	0.8506	3	29052	1790	358.1	20.7
1	113.4	567	72	0.6050	−0.3060	0.7351					

Table 4 Application examples summary

Example	Solution type, thrust	Transfer type, duration	Possible thrust directions, number of pseudoimpulses	Partial derivatives dependence on segment duration	Segment range	Number of segments	Number of decision variables	Number of nonzero decision variables in linear programming solution	Number of maneuvers after postprocessing	Number of boundary conditions	Interior-point constraints
Orbit maintenance	Station-keeping in vicinity of reference orbit, low-thrust	Many revolutions, 30 days	In plane, 36	Linear	10 deg in true anomaly	1080	38,880	~900	~60	6	Yes
GTO to GEO-transfer	Iterative solution for partial derivatives, low-thrust	Many revolutions, 29 days	In plane, 360	Nonlinear	Burn arc	80	28,880	46	46	3	——
Noncoplanar transfer between elliptical orbits	Iterative solution for partial derivatives, medium-thrust	One revolution, ~8.6 h	In three-dimensional space, 1000	Linear	10 deg in argument of latitude	72	72,000	17	3	4	——

where $\alpha = \alpha_p$ and $\sigma = -1$ (for the perigee) or $\alpha = \alpha_a$ and $\sigma = +1$ (for the apogee); $p = a_{i-1}(1 - e_{i-1}^2)$ is the orbit parameter; $R_e = 6378.14$ km is the mean equatorial radius of the Earth; $J_2 = 0.00108263$ is the Earth's oblateness coefficient; and $\omega = \sqrt{\mu/a_{i-1}^3}$ is the mean motion.

The transfer time corresponds to 40 revolutions. We assume 72 pseudoimpulses in each segment. Because the orbital elements for an intermediate transfer orbit are not known, we use an iterative solution. Linear dependences between the initial and target orbit elements were used as an initial guess for computation of the partial derivatives from Eqs. (25–27). Contrary to the previous example, the partial derivatives are nonlinear functions of a burn duration and therefore required a refinement in the iterative process (involving not only orbital elements, but the angles α_p and α_a for the burns with a nonmaximal duration). Time histories of a, e, and I are presented in Fig. 9 for the initial guesses (thin solid lines) and final solution after four iterations (bold solid lines). Note that the solution and solutions for other orbital transfers show that, as a rule, most of the burns have the maximal duration. As an illustration, a distribution of the burns for the orbit transfer is presented in Fig. 10. The total characteristic velocity ΔV_x is 1.317 km/s with ~29-day trip for this transfer, compared with optimal two-impulse transfer $\Delta V_x = 1.246$ km/s.

C. One-Revolution Orbit Transfer Between Elliptical Orbits

The presented method can be used to optimize of noncoplanar orbit transfers between two elliptical orbits with an unspecified number of burns. The thrust acceleration is assumed constant, equal to $a_p = 2 \times 10^{-4}$ km/s^2. The initial and target orbit parameters are shown in Table 2.

The one-revolution transfer was discretized into 72 segments with a uniform distribution in the argument of latitude and used a uniform distribution of the pseudoimpulses on a unit sphere with $k = 1000$ points. For an ith segment and jth pseudoimpulse the partial derivatives based on Gauss's form of the variational equations [22] can be expressed as

$$\frac{\partial a}{\partial V_i^{(j)}} = \frac{2a_i^2}{h_i}\left[e_i \sin(\vartheta_i) e_r^{(j)} + \frac{P_i}{r_i} e_n^{(j)}\right] a_p \Delta t_i \tag{31}$$

$$\frac{\partial I}{\partial V_i^{(j)}} = \frac{r_i \cos(U_i)}{h_i} e_b^{(j)} a_p \Delta t_i \tag{32}$$

$$\frac{\partial e}{\partial V_i^{(j)}} = \frac{1}{h_i}\{p_i \sin(\vartheta_i) e_r^{(j)} + [(p_i + r_i)\cos(\vartheta_i) + r_i e_i] e_n^{(j)}\} a_p \Delta t_i \tag{33}$$

$$\frac{\partial \omega_\pi}{\partial V_i^{(j)}} = \left(\frac{1}{h_i e_i}\{-p_i \cos(\vartheta_i) e_r^{(j)} + [(p_i + r_i)\sin(\vartheta) e_{ni}^{(j)}]\} - \frac{r_i \sin(U_i)\cos(I_i)}{h_i \sin(I_i)} e_b^{(j)}\right) a_p \Delta t_i \tag{34}$$

where $e_r^{(j)}$, $e_n^{(j)}$ and $e_b^{(j)}$ are the radial, along-track, and cross-track elements of the unit vector for the jth pseudoimpulse. The partial derivatives are linear functions of a segment duration.

The parameters of the initial orbit were used as an initial guess for the computation of the partial derivatives from Eqs. (31–34). The histories of the orbital elements after each iteration are shown in Figs. 11–14. The final solution after three iterations is depicted by bold lines. The numerical data of the final linear programming solution and results of the postprocessing to the burns are presented in Table 3.

In fact, it is a three-burn orbit transfer. The required variations of the thrust directions at each burn ($\Delta\gamma$, the last row in Table 3) are minor and correspond to thrust vector angular rates on the order of $\sim 1 \times 10^{-2}$ deg/s.

D. Examples Summary

Major qualitative features of the presented solutions are given in Table 4. The examples demonstrate a wide range of opportunities of for large-scale linear programming based on interior-point algorithms for optimization of continuous thrust orbit transfers.

V. Conclusions

In this paper, we have developed new optimization methods for continuous thrust orbit transfers, including medium- and low-thrust. The methods is based on a discretization of the trajectory dynamics on segments and a key idea is an extension for a space of the possible thrust directions by a set of pseudoimpulses for each segment. On the one hand it greatly increased the number of decision variables, but it also permitted a transformation of a nonlinear continuous orbit transfer problem to a classical linear programming form. We believe that the key idea can be applied to other nonlinear optimal control problems.

By a contrast with most traditional approaches of orbit transfer optimization where a total number of burns is often specified or constrained, the proposed technique has an attractive property related with an automatic computation of the burn number. Another attractive property is a possibility with the regard for operational constraints related with burn times and/or possible thrust directions. As an example, it can be an eclipse control where the electric engine is turned off whenever a spacecraft is in the Earth's shadow. The technique may also be used as a part the spacecraft design process for determination of a minimum thrust acceleration for a set of orbit transfers.

The presented examples demonstrated that the methods are applicable to optimization for a wide range of medium- and low-thrust orbit transfers.

Acknowledgment

The author thanks the Associate Editor, Robert Melton, for constructive comments and help in preparation of the paper.

References

[1] Melton, R. G., Lajoie, K. M., and Woodburn, J. W., "Optimum Burn Scheduling for Low-Thrust Orbital Transfers," *Journal of Guidance, Control, and Dynamics*, Vol. 12, No. 1, 1989, pp. 13–18.

[2] Kluever, C. A., "Low-Thrust Orbit Transfer Guidance Using an Inverse Dynamics Approach," *Journal of Guidance, Control, and Dynamics*, Vol. 18, No. 1, 1995, pp. 187–189.

[3] Rauwolf, G. A., and Coverstone-Carrol, V. L., "Near-Optimal Low-Thrust Orbit Transfers Generated by a Genetic Algorithm," *Journal of Spacecraft and Rockets*, Vol. 33, No. 6, 1996, pp. 859–862.

[4] Coverstone-Carrol, V. L., "Near-Optimal Low-Thrust Trajectories via Micro-Genetic Algorithms," *Journal of Guidance, Control, and Dynamics*, Vol. 20, No. 1, 1997, pp. 196–198.

[5] Kechichian, J. A., "Reformulation of Edelbaum's Low-Thrust Transfer Problem Using Optimal Control Theory," *Journal of Guidance, Control, and Dynamics*, Vol. 20, No. 5, 1997, pp. 988–994.

[6] Kluever, C. A., "Simple Guidance Scheme for Low-Thrust Orbit Transfers," *Journal of Guidance, Control, and Dynamics*, Vol. 21, No. 6, 1998, pp. 1015–1017.

[7] Ulybyshev, Y. P., and Sokolov, A. V., "Many-Revolution, Low-Thrust Maneuvers in Vicinity of Geostationary Orbit," *Journal of Computer and System Sciences International*, Vol. 38, No. 2, 1999, pp. 255–261.

[8] Pollard, J. E., "Simplified Analysis of Low-Thrust Optimal Maneuvers," The Aerospace Corporation TR-2000 (8565)-10, El Segundo, CA, Aug. 2000, p. 39.

[9] Herman, A. L., and Spencer, D. B., "Optimal, Low-Thrust Earth-Orbit Transfers Using Higher-Order Collocation Methods," *Journal of Guidance, Control, and Dynamics*, Vol. 25, No. 1, 2002, pp. 40–47.

[10] Petropoulos, A., "Low-Thrust Orbit Transfers Using Candidate Lyapunov Functions with a Mechanism for Coasting," AIAA Paper 2004-5089, Aug. 2004.

[11] Haberkorn, T., Martinon, P., and Gergaud, J., "Low Thrust Minimum-Fuel Orbital Transfer: A Homotopic Approach," *Journal of Guidance, Control, and Dynamics*, Vol. 27, No. 6, 2004, pp. 1046–1060.

[12] Pontryagin, L. S., Boltyanskii, V. G., Gamkrelize, R. V., and Mishchenko, E. F., *The Mathematical Theory of Optimal Processes*, Wiley, New York, 1962, Chap. 2.

[13] Enright, P. J., and Conway, B. A., "Discrete Approximations to Optimal Trajectories Using Direct Transcription and Nonlinear Programming," *Journal of Guidance, Control, and Dynamics*, Vol. 15, No. 4, 1992, pp. 994–1002.

[14] Seywald, H., "Trajectory Optimization Based on Differential Inclusion," *Journal of Guidance, Control, and Dynamics*, Vol. 17, No. 3, 1994, pp. 480–487.

[15] Betts, J., "Survey of Numerical Methods for Trajectory Optimization," *Journal of Guidance, Control, and Dynamics*, Vol. 21, No. 2, 1998, pp. 193–207.

[16] Waespy, C. M., "Linear Programming Solutions for Orbital Transfer Trajectories," *Operations Research*, Vol. 18, No. 6, 1970, pp. 635–653.

[17] Lidov, M. L., "Mathematical Analogy Between Optimal Problems of Trajectory Correction and Navigation Measurements" (in Russian), *Cosmic Research (Translation of Kosmicheskie Issledovaniya)*, Vol. 9, No. 5, 1971, pp. 687–706.

[18] Petrov, B. N., and Bazhinov, I. K. (eds.), *Flight Navigation Providing of Orbital Complex "Salyt-6"—"Soyus"—"Progress"* (in Russian), Nauka, Moscow, 1985, Chap. 44.

[19] Wright, S., *Primal-Dual Interior Point Methods*, SIAM, Philadelphia, 1997, Chap. 2.

[20] Rao, S. S., and Mulkay, E. L., "Engineering Design Optimization Using Interior-Point Algorithms," *AIAA Journal*, Vol. 38, No. 11, 2000, pp. 2127–2132.

[21] Wright, M. H., "The Interior-Point Revolution in Optimization: History, Recent Developments, and Lasting Consequences," *Bulletin of the American Mathematical Society*, Vol. 42, No. 1, 2004, pp. 39–56.

[22] Battin, R. H., *An Introduction to the Mathematics and Methods of Astrodynamics*, AIAA, New York, 1999, Chaps. 9.4, 10.3.

[23] *MATLAB® Users Guide*, Math Works, Natick, MA, 2003, Chap. 16.

[24] Lawden, D. F., *Optimal Trajectories for Space Navigation*, Butterworths, London, 1963, Chap. 5.

[25] Edelbaum, T. N., "Fifth and Sixth Integrals for Optimum Rocket Trajectories in a Central Field," *AIAA Journal*, Vol. 8, No. 7, 1970, pp. 1201–1204.

[26] Prussing, J. E., "Equation for Optimal Power-Limited Spacecraft Trajectories," *Journal of Guidance, Control, and Dynamics*, Vol. 16, No. 2, 1993, pp. 391–393.

[27] Bryson, A. E., Jr., and Ho, Y.-C., *Applied Optimal Control*, Hemisphere, New York, 1975, Chap. 7.3.

[28] Briskman, R. D., and Prevaux, R. J., "S-DARS Broadcast from Inclined, Elliptical Orbits," IAF Paper IAF-01-M.5.04, 2001, p. 20.

[29] Marsh, J. G., Lerch, F. J., Putney, B. H., Felsentreger, T. L., Sanchez, B. V., Klosko, S. M., Patel, G. B., Robbins, J. W., "The GEM-T2 Gravitational Model," *Journal of Geophysical Research*, Vol. 95, No. B13, 1990, pp. 22043–22071.